

# ONE-ARMED SPIRAL INSTABILITY IN A LOW $T/|W|$ POSTBOUNCE SUPERNOVA CORE

CHRISTIAN D. OTT<sup>1</sup>, SHANGLI OU<sup>2</sup>, JOEL E. TOHLINE<sup>2</sup>, AND ADAM BURROWS<sup>3</sup>

*Accepted by ApJL; AEI-2005-021*

## ABSTRACT

A three-dimensional, Newtonian hydrodynamic technique is used to follow the postbounce phase of a stellar core collapse event. For realistic initial data we have employed post core-bounce snapshots of the iron core of a 20  $M_{\odot}$  star. The models exhibit strong differential rotation but have centrally condensed density stratifications. We demonstrate for the first time that such postbounce cores are subject to a so-called low- $T/|W|$  nonaxisymmetric instability and, in particular, can become dynamically unstable to an  $m = 1$  - dominated spiral mode at  $T/|W| \sim 0.08$ . We calculate the gravitational wave (GW) emission by the instability and find that the emitted waves may be detectable by current and future GW observatories from anywhere in the Milky Way.

*Subject headings:* hydrodynamics - instabilities - gravitational waves - stars: neutron - stars: rotation

## 1. INTRODUCTION

Rotational instabilities are potentially important in the evolution of newly-formed proto-neutron stars (proto-NSs). In particular, immediately following the pre-supernova collapse – and accompanying rapid spin up – of the iron core of a massive star, nonaxisymmetric instabilities may be effective at redistributing angular momentum within the core. By transferring angular momentum out of the centermost region of the core, nonaxisymmetric instabilities could help explain why the spin periods of newly formed pulsars are longer than what one would expect from standard stellar evolutionary calculations that do not invoke magnetic field action for angular momentum redistribution and generation of very slowly rotating cores (Heger et al. 2000, Hirschi et al. 2004, Heger et al. 2004). Alternatively, in situations where the initial collapse “fizzles” and the proto-NS is hung up by centrifugal forces in a configuration below nuclear density, a rapid redistribution of angular momentum would facilitate the final collapse to NS densities. The time-varying mass multipole moments resulting from nonaxisymmetric instabilities in proto-NSs may also produce GW signals that are detectable by the burgeoning, international array of GW interferometers. The analysis of such signals would provide us with the unprecedented ability to directly monitor the formation of NSs and, perhaps, black holes.

In this Letter, we present results from numerical simulations that show the spontaneous development of a spiral-shaped instability during the postbounce phase of the evolution of a newly formed proto-NS. These are the most realistic such simulations performed, to date, because the pre-collapse iron core has been drawn from the central region of a realistically evolved 20  $M_{\odot}$  star, and the collapse of the core as well as the postbounce evolution has been modeled in a dynamically self-consistent manner. Starting from somewhat

simpler initial states, other groups have followed the development of bar-like structure in postbounce cores using Newtonian (Rampp et al. 1998) and relativistic (Shibata & Sekiguchi 2005) gravity, but their analyses have been limited to cores having a high ratio of rotational to gravitational potential energy,  $\beta \equiv T/|W| \gtrsim 0.27$ . We demonstrate that a one-armed spiral (not the traditional bar-like) instability can develop in a proto-NS even if it has a relatively low  $T/|W| \sim 0.08$ . This is significant, but perhaps not surprising given the recent studies by Centrella et al. (2001), Shibata et al. (2002, 2003), and Saijo et al. (2003).

## 2. NUMERICAL SIMULATION

The results presented in this Letter are drawn from three-dimensional hydrodynamic simulations that follow approximately 130 ms of the “postbounce” evolution of a newly forming proto-NS. Before presenting the details of these simulations, however, it is important to emphasize the broader evolutionary context within which they have been conducted and, specifically, from what source(s) the initial conditions for the simulations have been drawn. The two simulations presented here cover the final portion (Stage 3) of a much longer, three-part evolution that also included: (Stage 1) the main-sequence and post-main-sequence evolution of a spherically symmetric, 20  $M_{\odot}$  star through the formation of an iron core that is dynamically unstable toward collapse; and (Stage 2) the axisymmetric collapse of this unstable iron core through the evolutionary phase at which “bounces” at nuclear densities.

Stage 1 of the complete evolution was originally presented as model “S20” by Woosley & Weaver (1995). The initial configuration for this model was a chemically homogeneous, spherically symmetric, zero-age main-sequence star with solar metallicities. Evolution up to the development of an unstable iron core took some  $2 \times 10^7$  yr of physical time. In Stage 2 the spherically symmetric model from Stage 1 was mapped onto the two-dimensional, axisymmetric grid of the hydrodynamics code “VULCAN/2D” (Livne 1993) and evolved as model “S20A500/0.2” by Ott et al. (2004). Rotation was introduced into the core with a radial angular velocity profile  $\Omega(\varpi) = \Omega_0[1 + (\varpi/A)^2]^{-1}$  (where  $\varpi$  is the cylindrical radius). The scale length in the initial rota-

<sup>1</sup> Max-Planck-Institut für Gravitationsphysik, Albert-Einstein-Institut, Am Mühlenberg 1, 14476 Golm, Germany; cott@aei.mpg.de

<sup>2</sup> Center for Computation & Technology, Department of Physics & Astronomy, Louisiana State University, Baton Rouge, LA 70803

<sup>3</sup> Steward Observatory & the Department of Astronomy, The University of Arizona, Tucson, AZ 85721

tion law was set to  $A = 500$  km, and  $\Omega_0 = 3.36$  rad s $^{-1}$  was chosen so that, initially,  $\beta = 0.0020$ . The axisymmetric collapse was modelled adiabatically but the full Lattimer–Swesty equation of state (LSEOS; Lattimer & Swesty 1991) was incorporated.

During Stage 2, the innermost region of the unstable iron core collapsed homologously and, in  $\approx 0.5$  s, reached nuclear densities. As a consequence of angular momentum conservation, the core spun up considerably; at the time of the bounce, the rotational energy parameter had increased to  $\beta_b = 0.0896$ . As a result, the core bounce was aided as much by increased centrifugal forces as it was by the rapidly stiffening equation of state at nuclear densities. After bounce, the core expanded coherently, leading to almost an order-of-magnitude drop in the maximum density. This expansion was then reversed when gravitational forces again began to dominate over pressure gradients and centrifugal forces. In this way, the rapidly spinning, postbounce core underwent several damped-harmonic-oscillator like cycles. Ott et al. (2004) followed the axisymmetric evolution of model *S20A500 $\beta$ 0.2* for  $\sim 140$  ms after the time of its initial bounce,  $t_b$ .

In order to study the possible development of nonaxisymmetric structure in a newly forming proto-NS, we mapped the VULCAN/2D model into the fully three-dimensional hydrodynamic code FLOW•ER (Motl et al. 2002; Stage 3). In this work, we have adopted an ideal-fluid EOS:  $p = (\Gamma - 1)\epsilon\rho$ , where  $\rho$  is the mass density,  $p$  is the pressure,  $\Gamma$  is the chosen adiabatic exponent, and  $\epsilon$  is the specific internal energy. For sub-nuclear density matter — specifically, for  $\rho < \rho_{\text{nuc}} \equiv 2 \times 10^{14}$  g cm $^{-3}$  —  $\Gamma$  is set to 1.325, which approximates the  $\Gamma$  given by the LSEOS in VULCAN/2D in the sub-nuclear density regime and the given conditions. For  $\rho > \rho_{\text{nuc}}$ , we have set  $\Gamma = 2.0$  to mimic the effects of nuclear repulsive forces. FLOW•ER’s uniform cylindrical grid was constructed in such a way that it enclosed the innermost 140 km of model *S20A500 $\beta$ 0.2*, containing around  $1.4 M_\odot$  ( $\sim 75\%$  of the mass that was on the VULCAN/2D grid at the postbounce stage). Model *S20A500 $\beta$ 0.2* was mapped onto FLOW•ER’s grid at two different times during its postbounce evolution: Model “**Q15**” was evolved on a grid with (98, 128, 194) zones in  $(\varpi, \phi, Z)$  and mapped at  $t - t_b = 15$  ms when the core was in the middle of its second postbounce expansion phase. Upon introduction into the three-dimensional code, its density field was perturbed with an 0.1% amplitude, bar-like  $m = 2$  seed. Model “**W5**” was evolved on a higher resolution (130, 256, 194) grid, beginning at  $t - t_b = 5$  ms when the model reached its first density minimum after bounce. Random perturbations of 0.02% amplitude were imposed on the densities at mapping. Both models were evolved up to a time  $t - t_b \approx 130$  ms.

### 3. RESULTS

The key results of our three-dimensional evolutions are displayed in Fig. 1 (for model **Q15**) and Fig. 2 (for model **W5**). In the top panel of each figure, the time-dependent behavior of the global dipole ( $m = 1$ ; solid curve) and quadrupole ( $m = 2$ ; dotted curve) moments (Saijo et al. 2003) are plotted to illustrate how, and on what timescale, nonaxisymmetric structure developed. The time-dependent behavior of the rotational energy

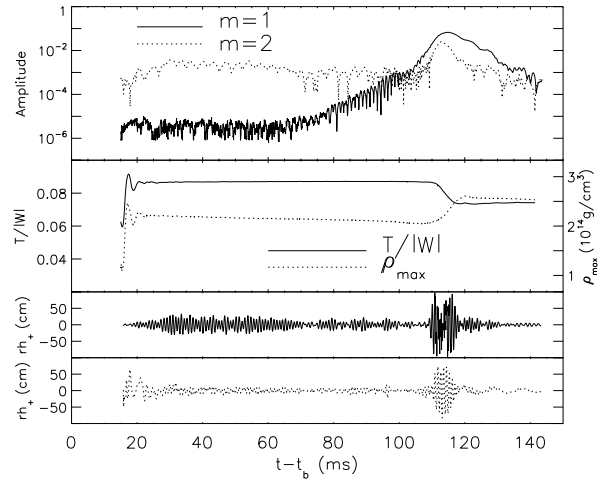


FIG. 1.— Time-evolution of various physical quantities is shown for model **Q15**; time (in ms) is given relative to  $t_b$ . Top: Globally-averaged amplitude of  $m = 1$  (solid curve) and  $m = 2$  (dotted curve) distortions. Middle: The rotational energy ratio  $\beta$  (solid curve) and the core’s maximum density  $\rho_{\text{max}}$  (dotted curve). Bottom: Product of the GW strain  $h_+$  and the distance to the source  $r$  as viewed down the rotation ( $z$ ) axis (solid curve) and as viewed along the  $x$ -axis (dotted curve).

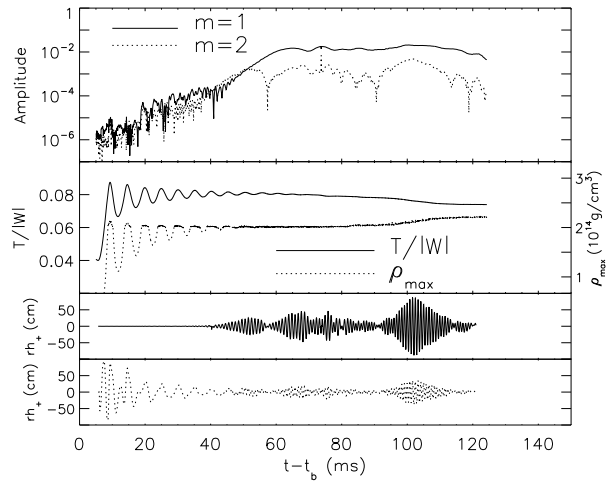


FIG. 2.— Same as Fig. 1, but for model **W5**.

parameter,  $\beta$  (solid curve), and the core’s maximum density,  $\rho_{\text{max}}$  (dotted curve), are shown in the middle section of the figures. The bottom third of each figure displays the amplitude of the gravitational radiation that would be emitted from each model as estimated by the post-Newtonian quadrupole formalism (see, e.g., Misner et al. 1973); specifically, for each model the time-dependent behavior of the product of the “plus polarization”  $h_+$  of the GW strain and the source distance  $r$  is shown as seen by an observer looking down the rotation axis (solid curve) or perpendicular to that axis (dotted curve). For a core-collapse event at  $r = 10$  kpc, an amplitude  $rh_+ = 100$  cm translates into  $h_+ = 3.2 \times 10^{-21}$ .

Because nonaxisymmetric perturbations were initially introduced into both models at a very low amplitude, the early phase of both evolutions resembled the axisymmetric evolution reported in Ott et al. (2004). Here, this is illustrated best by the oscillations in  $\beta(t)$  and  $\rho_{\text{max}}(t)$  that are shown in Fig. 2 for model **W5**; the characteristic (dynamical) time between successive “radial”

bounces is  $2\tau_{\text{dyn}} \sim 4$  ms (consistent with a mean core density  $\bar{\rho} \sim (\pi G \tau_{\text{dyn}}^2)^{-1} = 1.2 \times 10^{12} \text{ g cm}^{-3}$ ) and the axisymmetric oscillations persist for  $\sim 50$  ms. The curves of  $h_+(t)$  for model **W5** also signal that the dynamics is essentially axisymmetric: as viewed along the  $x$ -axis, the GW strain exhibits oscillations of diminishing amplitude, as reported in Ott et al. (2004), but for the first  $\sim 40$  ms after  $t_b$ , essentially no GW radiation is emitted along the  $z$ -axis. In model **Q15**, fewer “radial” bounces occur, they damp out somewhat more rapidly, and the resulting  $h_+(t)$  signal is weaker as viewed along the  $x$ -axis. This is, in part, because the postbounce core configuration was introduced into FLOW•ER at a later time ( $t - t_b = 15$  ms for model **Q15** instead of  $t - t_b = 5$  ms for model **W5**) and, in part, because the effects of numerical damping are inevitably more apparent when a simulation is run on a grid having lower spatial resolution. As is illustrated by the solid  $h_+(t)$  curves in the bottom panels of Figs. 1 and 2, at early times the amplitude of the gravitational radiation that would be emitted along the  $z$ -axis is larger in model **Q15** than in model **W5**. This reflects the fact that the nonaxisymmetric perturbation that was initially introduced into model **Q15** was larger and it had an entirely  $m = 2$  character.

Although in model **Q15** the postbounce core was subjected to a pure,  $m = 2$  bar-mode perturbation when it was mapped onto the FLOW•ER grid, the amplitude of the model’s mass-quadrupole distortion did not grow perceptibly during the first 100 ms ( $\sim 50$  dynamical times) of the model’s evolution (Fig. 1). However, as the solid curve in the same figure panel shows, the model spontaneously developed an  $m = 1$  “dipole” distortion even though the initial density perturbation did not contain any  $m = 1$  contribution. As early as  $t - t_b \approx 70$  ms, a globally coherent  $m = 1$  mode appeared out of the noise and grew exponentially on a timescale  $\tau_{\text{grow}} \approx 5$  ms. At  $t - t_b \approx 100$  ms, the amplitude of this  $m = 1$  distortion surpassed the amplitude of the languishing  $m = 2$  structure and, shortly thereafter, it became nonlinear. At  $t - t_b \approx 100$  ms, the quadrupole distortion also began to amplify, but it appears to have only been following the exponential development of the  $m = 1$  mode. An analysis of the oscillation frequency of both modes reveals them to be harmonics of one another. As the top panel of Fig. 2 illustrates, the same  $m = 1$  mode developed spontaneously out of the 0.02% amplitude, random perturbation that was introduced into model **W5**. The mode reached a nonlinear amplitude somewhat earlier in model **W5** than in model **Q15**, presumably because the initially imposed random perturbation included a finite-size contribution to an  $m = 1$  distortion whereas the density perturbation introduced into model **Q15** contained no  $m = 1$  component. The growth timescale of the instability is  $\tau_{\text{grow}} \approx 4.8$  ms for model **W5**. Although we have described the unstable  $m = 1$  mode as a “dipole” mass distortion, this is somewhat misleading because in neither model did the lopsided mass distribution produce a shift in the location of the center of mass of the system. Instead, as is illustrated in Fig. 3, the mode developed as a tightly wound, one-armed spiral, very similar to the  $m = 1$  - dominated structures that have been reported by Centrella et al. (2001) and Saijo et al. (2003).

After the spiral pattern reached its maximum ampli-

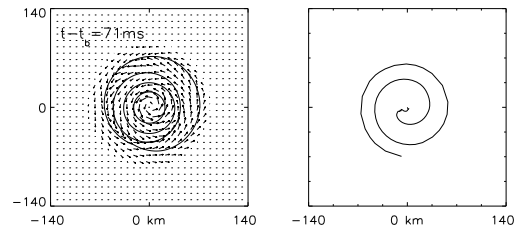


FIG. 3.— The equatorial-plane structure of model **W5** is shown at time  $t - t_b = 71$  ms. Left: Two-dimensional isodensity contours with velocity vectors superposed; contour levels are (from the innermost, outward)  $\rho/\rho_{\text{max}} = 0.15, 0.01, 0.001, 0.0001$ . Right: Spiral character of the  $m = 1$  distortion as determined by a Fourier analysis of the density distribution; specifically, the phase angle  $\phi_1(\omega)$  of the  $m = 1$  Fourier mode is drawn as a function of  $\omega$ .

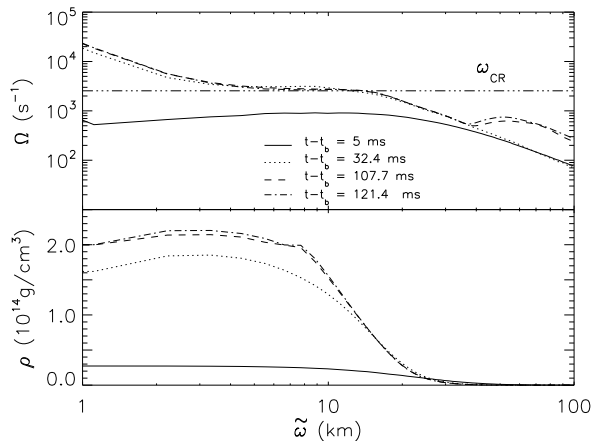


FIG. 4.— Equatorial-plane profiles of the azimuthally averaged angular velocity  $\Omega(\omega)$  (top frame) and the mass density  $\rho(\omega)$  (bottom frame) are shown at four different times during the evolution of model **W5**. Changes in these profiles at late times illustrate the effects of angular momentum redistribution by the  $m = 1$  spiral mode: angular momentum migrates radially outward while mass migrates radially inward. A horizontal line drawn in the top panel at  $\omega_{\text{CR}} = 2.5 \times 10^3 \text{ rad s}^{-1}$  identifies the corotation radius for this one-armed spiral mode. The “kink” seen in  $\rho(\omega)$  at late times at about 8 km is connected to the discontinuous switch of the EOS  $\Gamma$  at  $\rho_{\text{nuc}}$ .

tude in both of our model evolutions, the maximum density began to slowly increase and  $\beta$  started decreasing (Figs. 1 & 2). Following Saijo et al. (2003), we interpret this behavior as resulting from angular momentum redistribution that is driven by the spiral-like deformation and by gravitational torques associated with it. As angular momentum is transported outward, the centrifugal support of the innermost region is reduced, a larger fraction of the core’s mass is compressed to nuclear densities and, in turn,  $\beta$  decreases because the magnitude of the gravitational potential energy correspondingly increases. Fig. 4 supports this interpretation. As the proto-NS evolves, we see that the outermost layers spin faster and the innermost region becomes denser. (We note that throughout the evolution our models conserved total angular momentum to within a few parts in  $10^4$ .) Also, as is shown in the top panel of Fig. 4, throughout most of the model’s evolution there is a radius inside the proto-NS ( $\omega_{\text{CR}} \approx 12$  km) at which the angular velocity of the fluid matches the angular eigenfrequency ( $\omega_{\text{CR}} = 2.5 \times 10^3 \text{ rad s}^{-1}$ ) of the spiral mode. Hence, it is entirely reasonable to expect that resonances associated with this “corotation” region are able to effect a redis-

tribution of angular momentum in the manner described by Contopoulos (1980) or Watts et al. (2005).

Finally, we note that an off-center density maximum shows up at intermediate times, but since it is within the innermost radial grid zones, we are not sure if it is physical or an artifact due to the boundary conditions at the axis.

#### 4. SUMMARY AND DISCUSSION

Using the 3D, Newtonian, hydrodynamic code FLOW•ER, we have modelled the postbounce phase of the evolution of an iron core from an evolved, 20  $M_{\odot}$  star. In our first simulation (model **Q15**), the rotating core was mapped from two dimensions onto the three-dimensional grid at  $t - t_b = 15$  ms and the core's axisymmetric structure was altered by the introduction of a 0.1% amplitude, barlike density perturbation. The core was found to be dynamically stable to this pure  $m = 2$  perturbation, but it proved to be dynamically unstable toward the spontaneous development of a tightly wound,  $m = 1$  spiral mode. In an effort to examine the robustness of this result, we performed a second simulation (model **W5**) in which the rotating core was mapped at an earlier time ( $t - t_b = 5$  ms), onto a grid with higher spatial resolution, and the core's axisymmetric structure was altered by adding a lower-amplitude (0.02%) and *random* density perturbation. The  $m = 1$  spiral mode developed spontaneously in this model as well. Hence, we conclude that even relatively slowly rotating proto-NSs can be susceptible to the development of a spiral-shaped,  $m = 1$  - dominated mass distortion.

Although the nonaxisymmetric distortions that developed in both our models did not grow to particularly large nonlinear amplitudes, they produced maximum GW amplitudes comparable to the “burst” signal produced by the preceding, axisymmetric core collapse: Model **Q15** showed the highest amplitude,  $rh_{+, \max} \approx 100$  cm at a frequency  $f \approx 800$  Hz. The peak amplitude of the axisymmetric bounce signal reported in Ott et al. (2004) was  $rh_{+, \max} \approx 300$  cm at a frequency  $f \approx 400$  Hz. If the source is located within the Milky Way, both “burst” signals may be detected by the currently operative GW observatories (Ott et al. 2004). In our simulations, approximately 100 ms separated the peaks of these two GW “bursts,” but the earlier peak near  $t = t_b$  would, in practice, be unobservable if the rotation axis of the proto-NS were oriented along our line of sight, as is likely to be the case for core collapse events associated with gamma-ray bursts.

Our results demonstrate that a realistic, non-equilibrium postbounce stellar core can become dynamically unstable to an  $m = 1$  spiral instability at a value of  $\beta$  as low as  $\sim 0.08$ . (In model **W5**, this corre-

sponds to a spin period of 15 milliseconds at the surface of the proto-NS.) The value obtained in previous studies (Centrella et al. 2001, Saijo et al. 2003) for differentially rotating *equilibrium* models with a considerably simpler thermodynamic structure was  $\beta \sim 0.14$ . Saijo et al. (2003) argue that the growth of the instability in their models requires a soft EOS with effective  $\Gamma \lesssim 1.4$ . Our models exhibit an effective  $\Gamma$  just above this threshold while going unstable at lower  $\beta$ . This difference is most probably caused by the more complicated thermodynamic and rotational structure of our models. Most significantly, the instability in our low- $T/|W|$  models appears to be related to the proto-NS's angular velocity profile  $\Omega(\varpi)$ . Therefore, unlike the classical bar-mode instability that becomes unstable above a critical value of  $T/|W|$ , the relative stability of this spiral mode seems likely to depend on the existence or absence of a corotation resonance within the star. A wider variety of model simulations will be required to properly examine the validity of this conjecture. Our simulations support the suggestion of Saijo et al. (2003) that a spiral-mode instability can be effective at redistributing angular momentum within a proto-NS. In so doing, the instability can spin down the bulk of the core and, simultaneously, assist contraction of the innermost regions toward higher mean densities.

The present study marks only one very early step in our understanding of rotational instabilities in proto-NSs. The models we have used were purely hydrodynamic and Newtonian and did not include neutrino production and radiative transfer, or any of a variety of other microphysics that is likely to be relevant to these astrophysical systems. Future, fully consistent simulations including all the relevant physics will be needed to provide more definitive answers to these questions of stability.

We are happy to thank L. Lindblom, I. Hawke, H. Dimmelmeier, D. Pollney, R. Walder and E. Seidel for helpful comments. This work was partially supported by National Computational Science Alliance (NCSA) under grant MCA98N043. A.B. received support from the Scientific Discovery through Advanced Computing (SciDAC) program of the Department of Energy, grant DE-FC02-01ER41184. J.E.T. acknowledges support from NSF grants AST-0407070 and PHY-0326311. S.O. was supported by the Center for Computation and Technology at LSU. The computations were performed on the LSU Superhelix cluster, on the Peyote cluster at the Albert Einstein Institute and on NCSA's Tungsten cluster. We thank the Center for Gravitational Wave Physics at Pennsylvania State University (supported by the NSF under cooperative agreement PHY01-14375) for organizing the workshop during which this collaboration was initiated.

#### REFERENCES

- Centrella, J., New, K., Lowe, L., & Brown, J. 2001, *ApJ*, 550, L193  
 Contopoulos, G. 1980, *A&A*, 81, 198  
 Heger, A., Langer, N., & Woosley, S. E. 2000, *ApJ*, 528, 368  
 Heger, A., Woosley, S. E., & Spruit, H. C. 2004, *astro-ph/0409422*  
 Hirschi, R., Meynet, G., & Maeder, A. 2004, *A&A*, 425, 649  
 Lattimer, J. M., & Swesty, F. D. 1991, *Nucl. Phys. A*, 535, 331  
 Livne, E. 1993, *ApJ*, 412, 634  
 Misner, C. W., Thorne, K. S., & Wheeler, J. A. 1973, *Gravitation* (San Francisco, U. S. A: Freeman)  
 Motl, P., Tohline, J. E., & Frank, J. 2002, *ApJS*, 138, 121  
 Ott, C. D., Burrows, A., Livne, E., & Walder, R. 2004, *ApJ*, 600, 834  
 Rampp, M., Müller, E., & Ruffert, M. 1998, *A & A*, 332, 969  
 Saijo, M., Baumgarte, T. W., & Shapiro, S. L. 2003, *ApJ*, 595, 352  
 Shibata, M., Karino, S., & Eriguchi, Y. 2002, *MNRAS*, 334, L27  
 —. 2003, *MNRAS*, 343, 619  
 Shibata, M., & Sekiguchi, Y. 2005, *Phys. Rev. D*, 71, 024014  
 Watts, A. L., Andersson, N., & Jones, D. I. 2005, *ApJ*, 618, L37  
 Woosley, S. E., & Weaver, T. A. 1995, *ApJS*, 101, 181